Influence of Induction Motor in Stability of Power System with High Penetration of Large-Scale PV

Abdulrhman Alshareef
Mithulananthan Nadarajah
School of Information Technology and Electrical Engineering
The University of Queensland
St Lucia, QLD 4072, Australia
a.alshareef@uq.net.au; mithulan@itee.uq.edu.au

Rakibuzzaman Shah
School of Science Engineering and Information Technology
Federation University Australia
Mt Helen, VIC 3353, Australia
m.shah@federation.edu.au

***Abstract*—Inverter-Based Energy Resources (IBERs) have become an ordinary portion of the generation mix in power systems. Furthermore, converter-based technology has come to dominate modern motor loads on the consumption side. This transition in components towards accommodating power electronic devices alters the dynamic response of the power system. This paper investigates the impact of these elements on the dynamic stability of the power system. Firstly, this study successes to optimize a suitable model for converter-based motor loads. Secondly, indices of transient and voltage stabilities are used to quantify the strength of the power system at different circumstances incorporating the induction motor loads. Finally, this analysis provides an insight into the mutual interactions between transient and voltage stabilities. It is concluded that converter-based motor loads improve the voltage recovery when compared with direct-connected induction motors. However, the system is vulnerable to transient stability with the proliferation of inverter-based motor loads when IBERs dominant in the generation mix.**

***Index Terms*--Inverter-Based Energy Resources, motor drive model, system strength, time-domain simulation, transient stability, voltage recovery.**

I. INTRODUCTION

The power electronics technology advancement helps to introduce significant changes in integrating equipment in an efficient way within power systems. On the generation side, it allows non-conventional generations (NCGs) such as wind, photovoltaic (PV) and others to join the generation fleet. However, power electronics devices introduce several changes into load characteristics. For instance, it is noticeable that many modern electrical appliances with motors (air conditioners, refrigerators, and washing machines) are equipped with converter-based motor drives. It has been reported in the literature that the proliferation of electronics-based equipment on both the generation and load sides may alter the dynamic characteristics of power systems. It is stated in [1] that the injection of the reactive current of NCGs (inverter-based generators) is limited to 1.2 times the rated current. Consequently, the Dynamic Voltage Support (DVS) provided to the system will be less, especially during sudden large disturbances which pose voltage issues in a NCG dominated system [2]. On the load side, inverter-based motor drives are gradually replacing direct-connected induction motors (DCIM) given the energy savings and their quiet operation and high controllability. It was found in [3] that, when compared with DCIMs, system stability improved with drive deployment due to the operational characteristics of drives during the voltage dip. Therefore, to avoid conservative outcomes, it is important to consider both motor drives and DCIMs in load modelling.

An innovative positive-sequence model of inverter-based motor drives was introduced and validated with other motor drive models in [4]. However, this innovative drive model was a user-defined model that is not available within the model libraries of commercial analysis tools. Therefore, this paper first optimizes the parameters of DCIMs to mimic the response of the proposed model in [4] and then proposes a suitable model of drives for the utilities to be used for time-domain simulation. The optimization process used the Genetic Algorithm (GA) in MATLAB®. This study also investigateds the impact of the penetration of motor drives and NCGs, namely, Large-Scale PV (LSPV) on the dynamic stability of power systems using time-domain simulation in PSS®E software tools. Finally, dynamic stability is quantified using technical indicators to evaluate different load combinations and PV penetrations.

The remainder of the paper is organized as follows. The theoretical background relating to the research, including system strength, is addressed in Section II. System modelling is introduced in Section III. In Section IV, the methodology used in this research is elaborated. The numerical results and discussion are presented in Section V. Major conclusions and the contributions of the research are highlighted in Section VI.

II. THEORITCAL BACKGROUND

A. System Strength

System strength is defined as: "*an umbrella term for a suite of interrelated factors that together contribute to power system*

978-1-7281-6611-7/20/$31.00 ©2020 IEEE

stability" [5]. This definition is extended to cover all types of power system stability. The integrated power system naturally provides supplementary services such as fault current and synchronizing torque to enhance the system strength and keep the operation intact after major disturbances. However, the advent of modern power electronics-based technologies in the generation, transmission and distribution sectors changes the characteristics of these supplementary services. Thus, the dynamic response of the power system is expected to be altered. To assess different aspects of power system stability and quantify the system strength, several technical indices are discussed in the literature, such as Transient Stability Index (TSI), Rate of Machines Acceleration (ROMA), Transient Potential Energy-Kundur (TPE-K), Transient Kinetic Energy (TKE), Critical Clearing Time (CCT), Rate of Change of Frequency (RoCoF), Critical Modal Damping Factor (MDF), System Loadability Index (SLI), Transient Voltage Severity Index (TVSI) and Voltage Recovery Index (VRI) [6]-[8]. In this study, two indices related to transient stability and voltage stability are chosen as technical indicators to evaluate system performance.

B. Technical Indicators

Voltage Recovery Index (VRI) [6]: VRI is used to measure the system strength from a voltage stability point of view. VRI partitions the voltage profile into samples and compares the value of every sample with certain ride-through criteria. If the sample values are higher than the criteria, VRI is rewarded with positive weighting and the weight will be closer to (+1) as the voltage recovers to the pre-fault value. If the sample values are lower than the criteria, VRI is penalized with negative weighting and the weight will be closer to (-1) as the voltage approches zero. A third possiblity is if the sample values equal the criteria. In this case, VRI will not be rewared nor penalized but it will be zero for that sample. A detailed description of VRI is given in [6] and the references therein. However, the mathematical expression of VRI is shown in (1)

$$VRI = \frac{1}{A}\sum_{j=1}^{M}\sum_{i=1}^{L}(\eta_{ji}^{+}P_{ji}^{VRI+} + \eta_{ji}^{-}P_{ji}^{VRI-}) \tag{1}$$

In (1), A is the total number of samples between fault clearing time (t_c) to final simulation time (t_f), M is the number of voltage constraints according to the criterion voltage, and L is the total number of samples per M. The terms $\eta_{ji}^{+}P_{ji}^{VRI+}$ and $\eta_{ji}^{-}P_{ji}^{VRI-}$ are the rewards and penalties terms. The VRI range is $-1 \le VRI \le 1$ and the closer VRI is to (+1) as the voltage recovers, the better. Fig. 1 demonstrates the voltage recovery for different values of VRI. Basically, this index evaluates voltage recovery for each individual bus. However, VRI is utilized in this research to capture the system strength with respect to voltage stability by assigning the minimum voltage recovery in all buses

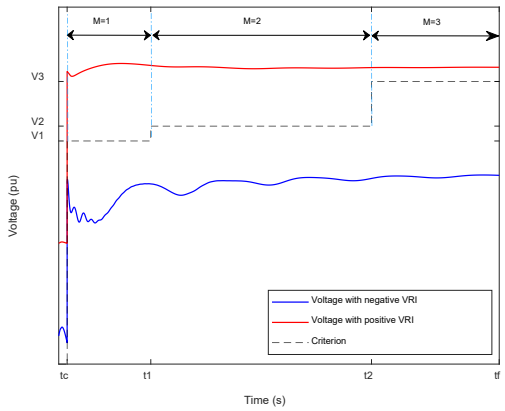

Fig. 1. Demonstration of different VRI values.

as voltage recovery of the entire system. Therefore, the system voltage recovery VRI_{sys} is expressed by (2).

$$VRI_{sys} = \min(VRI_1, VRI_2, ..., VRI_i) \tag{2}$$

In (2), i is the number of buses.

Transient Stability Index (TSI) [7]: TSI is used to measure the system strength from the transient (angular) stability perspective. The rotor angle of generators with respect to the reference generator is monitored to quantify the transient stability. TSI is defined in (3) and (4).

$$TSI = \frac{360^{\circ} - \delta_{\max}}{360^{\circ} + \delta_{\max}} \tag{3}$$

$$\delta_{\max} = \delta_i - \delta_{ref} \tag{4}$$

In (3)-(4), δ_i and δ_{ref} are the rotor angle of the i^{th} generator and the rotor angle of the reference generator, respectively. The value of TSI varies between 1 and -1 and TSI will be closer to 1 as the system is more stable. The system is considered unstable when $TSI < 0$ [10].

C. Genetic Algorithm

The Genetic Algorithm (GA) is a stochaistic optimization tool which searches for a global minimum value of a certain fitness function (e.g. an objective function to be minimized) subject to certain constraints [8]. GA was developed based on biological evolution to mimic chromosomal division in biological cells. A set of chromosomes (or 'individuals') forms a population and a set of populations is grouped as a generation. GA retains and improves the best individuals in each generation through selection, crossover, and mutation processes. The fitness function is evaluated for each generation and the production of new generations continues until the stopping criteria are met. The stopping criteria could be fitness limits, generation limits, stall generations, and time limits [9]. In this

research, GA is utilized to optimize the parameter model of DCIM to emulate the response of a motor drive under sudden large disturbances. This optimization process commenced by selecting the set of DCIM parameters and comparing the outcome response with the desired response of the motor drive. Based on the error between the two responses, GA changed the DCIM parameter sets until the stopping criteria is met.

III. SYSTEM MODELLING

A. Test System Model

Fig. 2 shows the test system used in this research. It represents a modified version of a reduced model of a realistic power system [10]. It contains 30 generator units distributed in four generation stations feeding a load of 4853 MW. Table I lists the generation stations data. Units at Gen_2, Gen_3, and Gen_4 stations are subjected to gradual decommissioning to accommodate the desired PV penetration level. Meanwhile, generators at Gen_1 station are kept committed for all cases, since Gen_1 is selected as a slack bus. The LSPV plants are considered to be part of the generation fleet of this system and the modelling of such is discussed next.

B. LSPV Plant Model

LSPV is modeled using the WECC generic model [6] and PV panels is aggregated and modelled as equivalent voltage sources as depicted in Fig. 3. The PV generation equivalent is linked with the following controllers from PSS®E library model: Generator/Converter (REGC_A) model, Electrical Control (REEC_B) model, and Plant Control (REPC_A) model. By adjusting the parameters of the controllers, the LSPV model can enable or disable the Dynamic voltage support (DVS). The calculation of the PV penetration level is expressed in (6).

$$PV \quad Penetration = \frac{\sum Gen_{PV}}{\sum Gen_{SG} + Gen_{PV}} \tag{6}$$

where Gen_{PV} and Gen_{SG} are the MW output of the PV plants and synchronous generators, respectively.

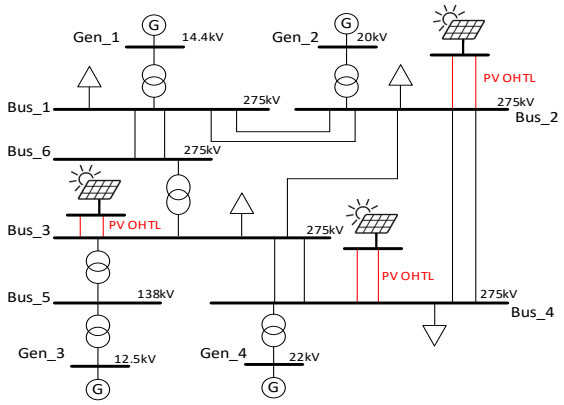

Fig. 2. Test system model [10].

TABLE I. GENERATOR DATA OF THE TEST SYSTEM

Gen. Station	Rated power (MVA)	No. of parallel machine	AVR model	Gov model
Gen_1	147.5	8	IEEET1	TGOV1
Gen_2	345.0	6	IEEEAC2	IEEEG1
Gen_3	115.5	9	IEEEST2	IEEEG1
Gen_4	455.0	7	EXPIC1	IEEEG1

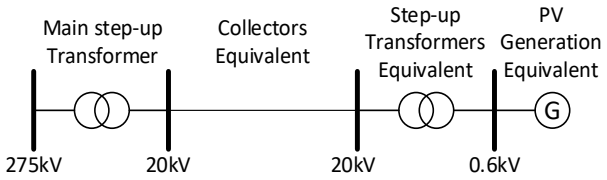

Fig. 3. LSPV plant model in PSS®E.

Different load models are accounted for in the test system, as discussed below.

C. Load Modelling

In a power system, loads are generally categorized as static and dynamic [11]. In this study, various combinations of these two categories are considered in the load representation. 50% of the total load is considered as dynamic for this study. The details of the two categories are discussed below.

Static Load Model: Static load representation in PSS®E is used to model half of the test system load. This model keeps the load as a constant MVA until a certain threshold is reached. When the terminal voltage of the static load drops beyond the threshold, an elliptical current-voltage characteristic, depicted in Fig. 4, is applied to modify the MVA load in PSS®E correspondingly [12]. Alternatively, a combination of static and dynamic loads can be used to represent the loads.

Dynamic Load Model: A third-order induction motor model, including the full model of rotor transient, is considered in this study. The swing equation of the rotor acceleration is expressed in (5).

$$\frac{d\omega_r}{dt} = \frac{1}{2H_{motor}}(T_e - T_m) \tag{5}$$

where H_{motor}, T_e, T_m, and ω_r refer to motor inertia, electrical torque, mechanical torque, and rotor angular speed, respectively [13]. The induction motor slip (S) and the reactive power consumption by the motor are calculated using real power (MW) and terminal voltage to initialize the model for time-domain simulation.

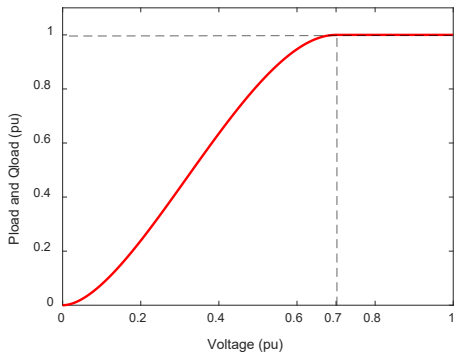

Fig. 4. Static Load Modelling in PSS®E.

Fig. 5 shows the equivalent circuit of a single-cage induction motor that is used to model the dynamic loads in this research. The dynamic load model is named CIM5BL in the PSS®E library [14]. Table II lists the the model's parameters.

IV. METHODOLOGY

Firstly, CIM5BL model parameters are optimized to mimic the motor drive response using GA. Then, different load models are incorporated into the test system with various levels of PV penetration to evaluate the system performance and establish the mutual interaction between voltage and transient stability through VRI and TSI indices.

A. Motor Drive Model Optimization

GA is used as an optimizer to tune the parameters of the CIM5BL model to identify the behavior of the motor drive in terms of voltage recovery, as reported in [4]. Single-cage CIM5BL model parameters for the rotor side, namely, X_m, R_1, X_1, H, and D, are used in the optimization process.

The fitness function shown in (7) is selected for this optimization process to ensure that the VRI at the motor drive terminal equals to 1.0.

$$minimize\,(1-VRI\,) \tag{7}$$

The procedure used in the optimization process is summarized in Fig. 5. At the end of that process, an appropriate dynamic model of the motor drive will be established using the PSS®E model library and utilized in the time-domain simulation.

B. Time-Domian Simulation

The test system is modelled in PSS®E with the dynamic models associated with the generators. The base case considered half the total load as static. In the initial scenario, the other half of the load is modelled as DCIMs.

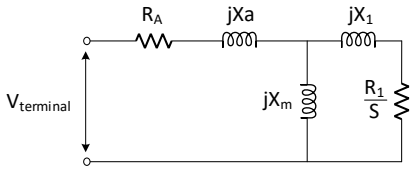

Fig. 5. Single-cage induction motor equivalent circuit.

TABLE II. SINGLE-CAGE CIM5BL MODEL PARAMETERS

Parameter (*pu*)	Description
R_a	Armature resistance
X_a	Armature inductance
X_m	Magnetizing inductance
R_1	Resistance of rotor winding
X_1	Reactance of the rotor winding
H	Inertia
D	Damping

DCIMs were then replaced, in steps of 5%, by the optimized motor drive model for each of the operational conditions. Next, a balanced fault is applied for 5-cycles as a disturbance for buses 1 to 6. Subsequently, the worst VRI_{sys} and TSI indices are recorded for all disturbances (fault locations).

The simulations are repeated for three different PV penetration levels, namely, 20%, 40% and 60%. A sub-total of 360 operational conditions are evaluated for conditions where DVS of LSPV are enabled. All scenarios were then repeated for situations where DVS of LSPV are disabled. A Total of 720 scenarios are checked for a variety of fault locations, load combinations, PV penetration and DVS of LSPV status. Finally, a batch of numerical results is produced and analyzed.

V. NUMERICAL RESULTS

A. Motor Drive Model Parameters

GA was successful in optimizing the motor drive model using the parameters shown in Table III. As shown in those parameters, inertia (H) is reduced to give a lighter reaction and higher acceleration after clearing the fault. The motor inertia (H) had strong impact on the acceleration and deceleration of the motor during starting, stopping and disturbance. Hence, the proposed reduction of motor inertia (H) reflects the decoupling nature of the motor drives from the network.

The block diagram of the CIM5BL model in the PSS®E manual [14] shows that the transfer function that relates motor speed (Δn) to electrical torque (T_e) is

$$\Delta n = \frac{\Delta T_e}{D_m + 2H_m s} = \frac{1}{D_m}\left(\frac{\Delta T_e}{1+(\frac{2H_m}{D_m})s}\right) \tag{8}$$

The time constant $\frac{2H_m}{D_m}$ governs the motor speed change. It is noticeable that the optimizer (GA) reduced this time constant by decreasing H_m and increasing D_m. Given this optimization

process, the recovery of motor drive terminal voltage with the optimized parameters of the CIM5BL model is shown in Fig. 7. It is clear that the voltage recovery with the optimized parameters approaches the target response. The target response in Fig. 8 represents the recovery of motor drives which can show instantaneous recovery due to the nature of decoupling from the network by the power electronic facilitator.

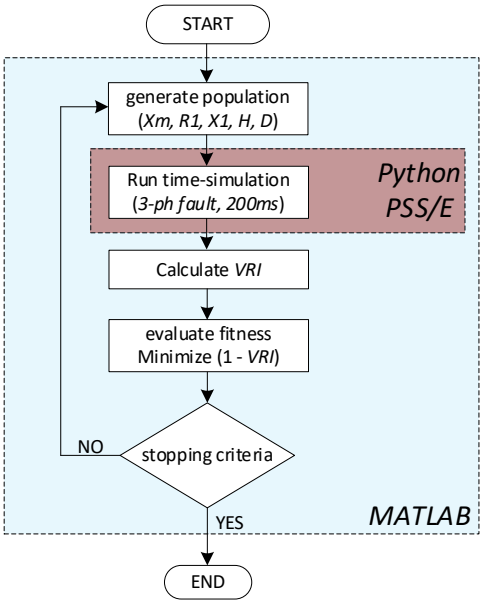

Fig. 6. Genetic Algorithm (GA) flowchart.

Next is to consider this optimized CIM5BL model with the load combinations and perform the time-domain simulation.

B. Time-domain simulation results

The described methodology of time-domain simulation is applied to the test system. Fig. 8 shows the trend of VRI_{sys} when more motor drives replaced DCIM at different PV penetration levels. For 20% and 40% PV penetration levels, it is clearly shown that VRI_{sys} improved rapidly when more motor drives replaced DCIMs. Conversely, at a 60% PV penetration level, VRI_{sys} remained constant until the percentage of motor drives reached 55% of the connected dynamic loads (point A in Fig. 8) and beyond this point, VRI_{sys} declined to low values.

TABLE III. CIM5BL MODEL PARAMETERS IN GA

	X_m	R_1	X_1	H, inertia	D	Fitness function
DCIM	4.0000	0.0400	0.2770	0.2800	2.0000	-
optimized	0.4707	0.0180	0.0182	0.0142	4.6311	0.003048

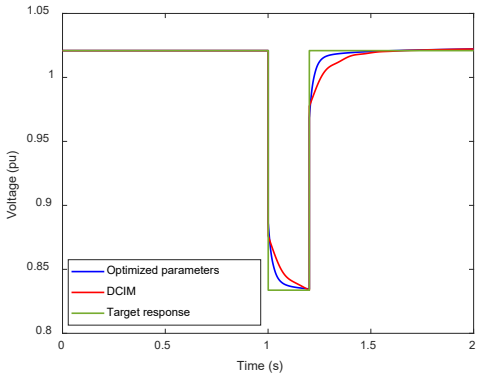

Fig. 7. Voltage Recovery with different parameters.

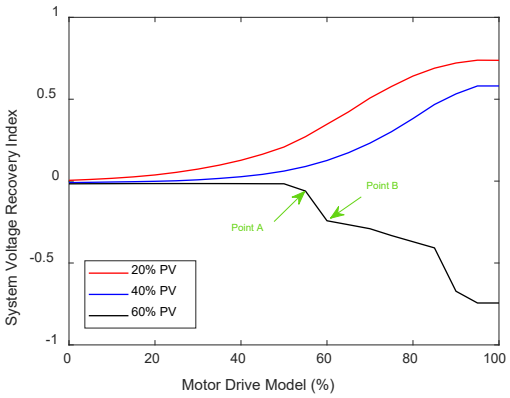

Fig. 8. VRI_{sys} with different penetration of PV and drives.

Note that the percentages on the x-axis represent the portion of the motor drive model that replaces the connected dynamic load DCIMs).

Fig. 9 compares VRI_{sys} with and without DVS of LSPV. It reflects that the possibility of enabling and disabling DVS has a similar overall trend of voltage recovery and that positively enabling DVS cases have healthier voltage recovery. In the disabling DVS mode, higher PV penetration levels will lead to weaker voltage recovery due to de-committing of SGs and disabling DVS of LSPV.

The TSI index for different PV penetration levels and motors drives is shown in Fig. 10. The TSI index almost constant for 20% and 40% PV penetration levels. However, at the 60% PV penetration level, TSI suddenly falls to the unstable region (less than zero) when more than 55% of the connected dynamic loads are comprised of motor drives. This behavior of TSI explains the VRI_{sys} collapse beyond point A in Fig. 9.

The time-domain simulation of machine angle depicted in Fig. 11 shows the transition of machine angle from stable to unstable status (points A and B in Fig. 8).

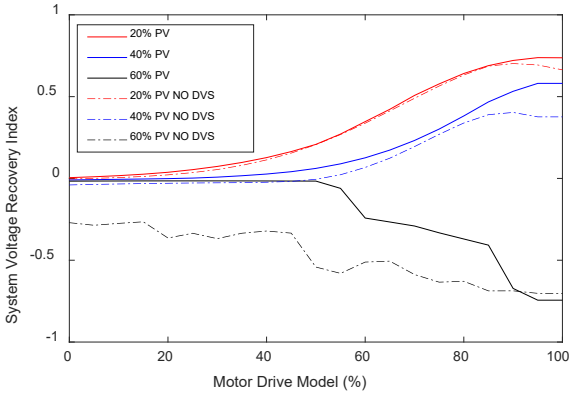

Fig. 9. VRI_{sys} with and without DVS.

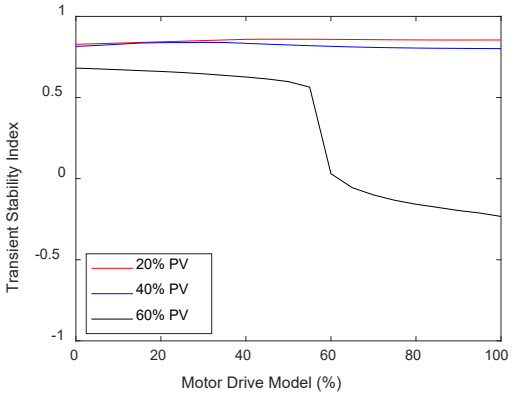

Fig. 10. TSI with different penetration of PV and drives.

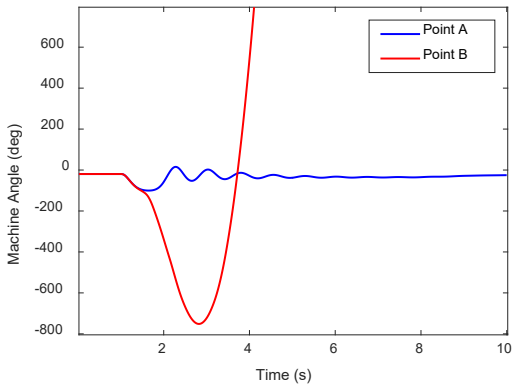

Fig. 11. Machine angle at points A&B.

VI. CONCLUSIONS

This paper identifies the impact of higher PV penetration levels on voltage recovery and system strength, considering different load model combinations. Firstly, higher PV penetration negatively impacted voltage recovery and system strength. Secondly, the existence of motor drives strengthened the system and improved voltage recovery compared with DCIMs to a certain PV penetration level. However, higher PV penetration levels make the system sensitive to the proliferation of motor drives. As a result, the system was vulnerable to transient instability issues. This situation was triggered by the rotational mass reduction on both the generation and load sides. Consequently, the rotor machine angles were unstable due to the lack of synchronizing torque in the system. Thirdly, this study also sheds light on the mutual impacts between transient and voltage stabilities. It consistently confirms that when the generators experience transient stability issues, the voltage will, indubitably, be unstable.

REFERANCES

[1] IEEE/NERC Task Force on Short-Circuit and System Performance, " Impact of Inverter Based Generation on Bulk Power System Dynamics and short-Circuit Performance," July 2018 2018.

[2] F. Milano, F. Dörfler, G. Hug, D. J. Hill, and G. Verbič, "Foundations and Challenges of Low-Inertia Systems (Invited Paper)," in *2018 Power Systems Computation Conference (PSCC)*, 11-15 June 2018 2018, pp. 1-25.

[3] Y. Liu and V. Vittal, "Distribution side mitigation strategy for fault induced delayed voltage recovery," in *2014 IEEE PES General Meeting | Conference & Exposition*, 27-31 July 2014 2014, pp. 1-5.

[4] Y. Liu and V. Vittal, "Modeling of Rectifier-Controlled Induction Motor Drive Load in Transient Stability Simulation Tools," *IEEE Transactions on Power Systems,* vol. 33, no. 5, pp. 4719-4729, 2018.

[5] A. E. M. O. (AEMO);, "Power system requirements," 2018.

[6] G. Lammert, D. Premm, L. D. P. Ospina, J. C. Boemer, M. Braun, and T. V. Cutsem, "Control of Photovoltaic Systems for Enhanced Short-Term Voltage Stability and Recovery," *IEEE Transactions on Energy Conversion,* vol. 34, no. 1, pp. 243-254, 2019.

[7] L. Shi, S. Dai, Y. Ni, L. Yao, and M. Bazargan, "Transient stability of power systems with high penetration of DFIG based wind farms," in *2009 IEEE Power & Energy Society General Meeting*, 26-30 July 2009 2009, pp. 1-6.

[8] R. Chaudhary, A. Shahpatel, and S. Patel, "Optimal design of Induction Motor using Genetic Algorithm and comparision with conventionally Designed Induction motor," in *2016 IEEE 1st International Conference on Power Electronics, Intelligent Control and Energy Systems (ICPEICES)*, 4-6 July 2016 2016, pp. 1-4.

[9] S. N. Sivanandam and S. N. Deepa, *Introduction to Genetic Algorithms*, 1st ed. 2008.. ed. Berlin, Heidelberg: Springer Berlin Heidelberg : Imprint: Springer, 2008.

[10] R. Shah, R. Preece, and M. Barnes, "The Impact of Voltage Regulation of Multiinfeed VSC-HVDC on Power System Stability," *IEEE Transactions on Energy Conversion,* vol. 33, no. 4, pp. 1614-1627, 2018.

[11] A. Adrees and J. Milanović, "Effect of load models on angular and frequency stability of low inertia power networks," *IET Generation, Transmission & Distribution,* vol. 13, no. 9, pp. 1520-1526, 2019.

[12] Siemens Industry Inc, "PSS/E Program Operation Manual."

[13] N. B. P Kundur, MG Lauby, *Power system stability and control*. 1994.

[14] Siemens Industry Inc, "Program Application Guide Volume 2 PSS®E 34.6.0," 2019.

978-1-7281-6611-7/20/$31.00 ©2020 IEEE